Flexible Polymer-Assisted Mesoscale Self-Assembly of Colloidal $CsPbBr_3$ Perovskite Nanocrystals into Higher Order Superstructures with Strong Inter-Nanocrystal Electronic Coupling

Yang Yang,[$,1] Jacob T. Lee,[$,1] Thakshila Liyanage,[1] and Rajesh Sardar*[1,2]

[1]Department of Chemistry and Chemical Biology, Indiana University-Purdue University Indianapolis, Indianapolis, Indiana 46202, United States

[2]Integrated Nanosystems Development Institute, Indiana University-Purdue University Indianapolis, Indianapolis, Indiana 46202, United States

Abstract: Surface passivating ligands, although ubiquitous to colloidal nanocrystal (NCs) synthesis, play a role in assembling NCs into higher-order structures and hierarchical superstructures, which has not been demonstrated yet for colloidal $CsPbX_3$, (X= Cl, Br, and I) NCs. In this work, we report that functional polyethylene glycols (PEG_6-Y, Y = -COOH and $-NH_2$) represent unique surface passivating ligands enabling the synthesis of near uniform CsPbBr3 NCs with diameters of 3.0 nm. The synthesized NCs are assembled into individual pearl necklaces, bundled pearl necklaces, lamellar, and nanorice superstructures, *in-situ*. It is believed a variety of forces, including van der Waals attractions between hydrophilic PEG tails in a nonpolar solvent and dipole-dipole attraction between NCs, drive mesoscale assembly to form superstructures. Furthermore, post-synthetic ligand treatment strengthens the argument for polymer-assisted mesoscale assembly as pearl necklace assemblies can be successfully converted into either lamellar or nanorice structures. We observe an ~240 meV bathochromic shift in the lowest energy absorption peak of $CsPbBr_3$ NCs when they are present in the lamellar and nanorice assemblies, representing strong inter-NC electronic coupling. Moreover, pearl necklace structures are spontaneously assembled into micrometer length scale twisted ribbon hierarchical superstructures during storage of colloidal $CsPbBr_3$ NCs. The results show that the self-assembled superstructures of $CsPbBr_3$ NCs are now feasible to prepare via template free synthesis, as self-assembled structures emerge in the bulk solvent, a process that mimics biological systems except for the use of non-biological surface ligands (PEG_6-Y). Taken together, emergent optoelectonic properties and higher-order superstructures of $CsPbBr_3$ NCs should aid their potential use in solid-state devices and simplify scalable manufacturing.

INTRODUCTION

Fascinating size and composition dependent optoelectronic properties,[1-3] interfacial charge transfer[4-6] along with improved colloidal stability of all-inorganic, highly ionic cesium lead bromide perovskite ($CsPbX_3$, X= Cl, Br, and I) nanocrystals (NCs) make them attractive candidates for solar-cells, light-emitting diodes, and lasing applications.[7-11] The high temperature hot injection method developed by Kovalenko and coworkers12 for the synthesis of $CsPbX_3$ NCs has prompted a new approach for the preparation of NCs of varying shapes (e.g., spherical, cubes, wires, and platelets). Currently, most synthetic methods produce an ordered-assembly of $CsPbX_3$ nanocubes, nanowires, and nanoplatelets.[12-23] These assemblies are formed mostly due to cooperative (dipole-dipole, hydrophobic, and van der Waals (vdW)) interactions between the long aliphatic chains of surface passivating ligands.[24-27] Recently, we reported that surface ligand chemistry profoundly impacts the self-organization of methylammonium lead bromide ($CH_3NH_3PbBr_3$) perovskite NCs, leading to stacked nanoplatelets and bundles of nanowires as hierarchically organized superstructures.[28, 29] The programmable assembly of either $CsPbX_3$ or $CH_3NH_3PbBr_3$ NCs into higher order superstructures via modification of surface ligand chemistry has not yet been demonstrated, but are important to the field in order to understand how these highly ionic NCs are electronically interacted inside the hierarchical superstructures that could lead to the fabrication of efficient solid-state devices.

In this work, we report the synthesis of flexible polymeric ligand-passivated cubic-phase and monodisperse $CsPbBr_3$ NCs with ~3.0 nm diameters, which are assembled into individual pearl necklaces, bundled pearl necklaces (~550 nm in length), close-packed, lamellar, and nanorice assemblies. To our knowledge, this is the first example in which a spontaneous self-assembly of polymer-passivated highly ionic inorganic NCs has resulted in one-dimensional, individual and bundled pearl necklaces without applying any external fields or preforming covalent attachment through template-free chemical and/or polymerization reactions.[30-37] Thermodynamically-driven, surface passivating ligand-controlled mesoscale assembly processes circumvent two technical challenges in order to prepare various assemblies of colloidal NCs, including metal and metal chalcogenide NCs: (1) avoiding widely adopted ligand exchange process and (2) performing additional chemical transformations. The *in-situ* self-assembly process of either fully inorganic or inorganic-organic hybrid perovskite NCs is important because these highly ionic NCs are extremely susceptible to undergo degradation in polar solvents and/or ionic environments that are required for ligand exchange, and chemical and/or polymerization reactions. Together, we also show that three important structural parameters (i.e., chain length, concentration, and binding head groups) of the flexible polymers are critically controlling the *in-situ* self-assembly process of $CsPbBr_3$ NCs that together promote the formation of higher order superstructures through a combination of cooperative interactions between individual polymer-passivated NCs.

Developing unique surface ligand chemistry capable of organizing NCs into complex and higher order structures through self-assembly opens new possibilities of achieving emergent optoelectronic and electrical properties at the nanoscale that are different from the individual components. Polymeric materials are frequently used for embedding NCs over multiple length scales through self-assembly processes.[33, 38-42] Moreover, inter-NC interaction can be controlled inside the polymer-NC organic-inorganic hybrid material superstructures, thus laying a foundation for preparation of the first perovskite-based artificial solids with unique functions. The optical band-gap (E_{op}) of $CsPbBr_3$ NCs in an individual pearl-necklace (E_{op} = 2.57 eV) is ~70 meV red-shifted compared to bundled pearl necklace (E_{op} = 2.64 eV) structures. Furthermore, lamellar and nanorice structures display the highest and lowest E_{op} of 2.70 and 2.46 eV, respectively, whereas NCs in close-packed self-assembly show E_{op} of 2.51 eV. Therefore, we hypothesize the overall 240 meV change in the E_{op} is due to inter-NC electronic coupling through excitonic wavefunction delocalization in the higher order structures.

Over the last three years, significant attention has been given to the production of fatty acid- and/or amine-passivated fully inorganic perovskite NCs through colloidal synthetic methods,[12, 43-46] however, less effort has been devoted on the use of surface ligand chemistry to control NC assemblies during synthesis. As mentioned above, since ligand exchange chemistry of $CsPbX_3$ NCs has not been explored yet, direct synthesis of perovskite NCs with unique surface passivating ligands is critical to appropriately functionalizing their surface and controlling inter-NC interactions. This should provide a unique opportunity to create various molecular interactions that result from the self-assembly of individual NC into higher order superstructures, which would then eventually promote charge transport efficiency of solid-state devices made with perovskite NCs, as this has well documented for metal chalocogenide NCs.[47-49]To prepare such higher order superstructures, functional polyethylene glycol (PEG_6-Y, Y = -COOH and NH_2)-passivated $CsPbBr_3$ NCs are synthesized at a moderately low temperature (~60 ^oC). We selected PEG_6-Y because acids and amines are known to interact with surface Pb and Br sites, respectively,[28, 50, 51] which in turn can provide colloidal stability and improved optoelectronic properties of $CsPbBr_3$ NCs. Additionally, the oxygen within the glycol units can datively interact with the Pb of $CsPbBr_3$ in order to wrap the NCs with flexible polymer chains similar to a *"meatball and spaghetti"* model.[52, 53] Finally, PEG is a hydrophilic polymer and thus thermodynamically favorable interactions between PEG chains on adjacent NCs in hydrophobic solvents should drive the self-assembly process. Utilizing these inherent properties of PEG, we are able to successfully transform individual pearl-necklaces structures into lamellar and nanorice structures through post-synthetic ligand treatment. Taken together, we propose that a combination of dipole-dipole interactions between $CsPbBr_3$ NCs and van der Waals (vdW) attraction between surface passivating ligands induce the mesoscale assembly of spherical NCs into individual and bundled pearl-necklaces, and lamellar structures. In addition to these two forces, ionic interactions between COOH and $–NH_2$ binding head groups of PEG_6 are responsible for the formation of nanorice structures. Finally, during storage of microscale pearl-necklace assemblies in colloidal suspension, twisted ribbon structures are spontaneously formed. Therefore, the current work on template-free synthesis of hierarchical superstructures could be compared with biological systems where nature produces many complex higher order structures. Moreover, such programmable transformation of NC assemblies, in particular perovskite NCs, has not yet been reported in literature. Additionally, various assemblies could be considered as "nanocomposites" that should provide two advantages (1) structural benefit of the polymer[52, 54] (flexible glycol units of PEG chains and ability to transport charge) as compared to NCs, which are passivated with small, insulating organic ligands; and (2) unique optoelectronic properties of $CsPbBr_3$ NCs.

Results and Discussion

Synthesis and Characterization of Flexible Polymer-Passivated Perovskite NCs. We synthesized PEG_6-NH_2 and PEG_6-COOH in our laboratory using literature procedures.[55, 56] Supporting Information file provides experimental procedure and ^{1}H NMR spectra (**Figure S1 and S2**). In our initial investigation, we use a mixture of PEG_6-NH_2 (0.2 millimole, mmol) and PEG_6-COOH (0.03 mmol) as surface passivating ligands in the synthesis of cesium lead bromide perovskite at 60 ^{O}C The purified perovskite material is soluble in chloroform, forming a yellow solution. Transmission electron microscopy (TEM) analysis of the product shows the presence of nearly monodispersed NCs with an average diameter of 3.0 ± 0.4 nm (**Figure 1A**). Furthermore, on the TEM grid the NCs are observed as a two-dimensional (2D) close-packed structure with an average 2.3 nm inter-NC spacing (**Figure S3**). As shown in the low-magnification TEM image (**Figure S4**) the 2D structures are micrometer-sized in dimension. Elemental analysis through energy dispersive X-ray spectroscopy (data not shown) confirms a

Cs:Pb:Br ratio of 1:1:3.1, confirming the formation of $CsPbBr_3$ NCs. **Figure 2** (Panel A) represents the X-ray diffraction (XRD) patterns of $CsPbBr_3$ NCs that correlates to a cubic structure (PDF# 84-0464). Interestingly, the XRD peaks of NCs are slightly shifted to lower angles; this can be related to strain in the lattice structure due to adsorption of -COOH and/or -NH_2 head group containing ligands, as previously shown for metal chalcogenide NCs.[57, 58] FTIR spectroscopy was used to characterize surface ligand chemistry. **Figure S5** exhibits the FTIR spectra of ligand-passivated $CsPbBr_3$ NCs and shows that the characteristic -C=O and -N-H stretches related to PEG_6-COOH and PEG_6-NH_2, respectively, are observed, confirming the NCs are mixed ligand passivated. Importantly, the FTIR spectra also indicate electronic interactions between the carboxylic acid group and NC, and not negatively charged PEG-COO^-.[59] The UV-visible absorption and narrow photoluminescence (PL) spectra of the synthesized $CsPbBr_3$ NCs display peaks at 494 nm (2.51 eV) and 504 nm (2.46 eV), respectively (**Figure 1B**). This 50 meV Stokes' shift can be related to surface defects. The appearance of a sharp absorption peak supports the narrow size distribution of $CsPbBr_3$ NCs. UV-visible absorption spectrum shows long tailing at longer wavelengths, indicating the presence of higher-order structures in solution further supporting the TEM analysis mentioned above. Importantly, ligand-passivated $CsPbBr_3$ NCs displaying the lowest energy, a sharp absorption peak at 2.51 eV, should correlate to a size of 6-8 nm in diameter, as reported in the literature both experimentally and theoretically.[12] In contrast, we observe nearly similar band-gap for our mixed PEG_6-COOH- and PEG_6-NH_2-passivated, 3.0 nm diameter $CsPbBr_3$ NCs. According to quantum confinement theory, ~3.0 nm diameter NCs should display larger band-gap than 2.51 eV. We hypothesize this deviation of the experimentally observed optical band gap from theory is a consequence of the delocalization of exciton (electron and/or hole) wavefunction of NCs, which increases the confinement box size and allows strong inter-NC electronic coupling. It has been reported that the "solvent-like" properties of PEGs allow strong inter-NC electronic coupling resulting from the delocalization of excitonic wavefunctions.[60] Furthermore, dipole-dipole interactions between NCs could also lead to red-shifts (bathochromic shifts) in the absorption peak. We discuss this interesting optoelectronic property below.

Polymer-Assisted Formation of Higher-Order Assemblies of $CsPbBr_3$ NCs and Their Optoelectronic Properties. As schematically shown in **Figure 3**, we explore the role of surface passivating ligands in the in-situ synthesis of $CsPbBr_3$ NCs by manipulating two reaction conditions: (i) use PEG_6-NH_2 only as an added ligand, and (ii) use both PEG_6-NH_2 and PEG_6-COOH as ligands, but increase the concentration of the latter component as compared to our initial studies. PEG_6-NH_2 concentrations in the reaction mixture were varied from 0.2 to 0.4 mmol. TEM characterization shows the formation of sub-micrometer length scale individual pearl necklaces, bundled pearl necklaces, and lamellar assembles of $CsPbBr_3$ NCs in the presence of just PEG_6-NH_2 as a surface passivating ligand (**Figure 4A-C**). In contrast, nanorice assemblies containing spherical $CsPbBr_3$ NCs form when both PEG_6-NH_2 and PEG_6-COOH are present (see **Figure 4D**). These higher order superstructures are made with a nearly identical size of ~3.0 nm diameter $CsPbBr_3$ NCs (see supporting Information for size analysis) with a cubic crystal phase (see **Figure 2**). Additional TEM images are provided in the Supporting Information, see **Figure S6-S9**. Importantly, we also attempt to synthesize $CsPbBr_3$ NCs in the presence of just PEG_6-COOH as ligands with relatively higher concentrations that results in an organically insoluble white solid. Use of higher concentrations of PEG_6-NH_2 in the synthesis provides a highly viscous yellow material, and we found it to be difficult to purify the NCs.

Utilizing the chemical structures of surface ligands, gold[31, 32, 34-37] and magnetic[30, 33] nanoparticles, and CdTe quantum dots[26] have been organized into one-dimensional chains (pearl necklace assembly). However, the work herein represents the first example in which polymer-passivated $CsPbBr_3$ NCs are organized into either individual or bundled pearl necklace assemblies. It should be noted that all the above-mentioned works on template-free synthesis of pearl necklace assembly of various nanoparticles require: (1) ligand exchange reaction to attach specific surface functionalization groups, which could covalently link to form one-dimensional structures; (2) living free-radical polymerization reaction to connect individual nanoparticles into a pearl necklace assembly.[61] In contrast, our PEG ligand-driven *in-situ* formation of pearl necklace assemblies of $CsPbBr_3$ NCs does not require polymerization and/or ligand exchange reactions, specifically circumventing the latter case that is found to be extremely challenging for perovskite NCs in general.[62] Particularly, ligand exchange reactions may not be as straightforward for perovskite NCs as compared to metal and metal oxide nanoparticles and metal chalocgenide quantum dots because there are several factors, such as concentration and binding head group of surface passivating ligands, and the solvent system that all control the exchange processes. Moreover, new ligand passivation may hinder the appropriate solubility property of NCs for complete ligand exchange in order for the self-assembly processes to take place. Then, stability of $CsPbBr_3$ NCs during the exchange reaction is another issue. Taken all the factors together, we believe that the demonstrated *in-situ* self-assembly process for $CsPbBr_3$ NCs should be applicable to prepare different assemblies of other ionic nanoparticles beyond perovskite NCs.

UV-visible spectroscopy characterizations of different assemblies of $CsPbBr_3$ NCs reveal non-size dependent optoelectronic properties. The E_{op} of lamellar, bundled and individual pearl necklace, close-packed, and nanorice structures are 460 nm (2.70 ev), 470 nm (2.64 eV), 483 nm (2.57 eV), 494 nm (2.51 eV) and 505 nm (2.46 eV), respectively (see **Figure 4E-H**). **Table 1** summarizes the assembly dependent optical properties of ~3.0 nm diameter $CsPbBr_3$ NCs under our optimized reaction conditions. Importantly, E_{op} of our ~3.0 nm diameter $CsPbBr_3$ NCs in lamellar assembly is in agreement with the E_{op} reported by Kovelenko group.[12] Surprisingly, the lowest band-gap (2.46 eV) observed for ~3.0 nm diameter $CsPbBr_3$ NCs is in the nanorice assembly, which is significantly red-shifted (~2.0 eV) as compared to the theoretical value of 4.46 eV for a discrete 3.0 nm $CsPbBr_3$ NC, as determined from effective mass approximation calculations.[63] Therefore, our $CsPbBr_3$ NCs behave more like bulk perovskite materials (E_{op} = 2.25 eV)[64] while maintaining nanoscale properties as similar to *"artificial solids"*. Moreover, as mentioned above, while all of these assemblies are made with nearly identical size, ~3.0 nm $CsPbBr_3$ NCs we observe a large difference in their E_{op}-gaps. Hence, we hypothesize that the ~240 meV bathochromic shifts in the lowest energy absorption peak between lamellar and nanorice assembly are due to delocalization of excitonic wavefunctions in the NCs that increase the confinement box size. The exciton binding energy of $CsPbBr_3$ NCs are relatively small (<100 meV).[65, 66] Moreover, kinetic energy of excitons (electrons and/or holes) within NCs at their relatively small size range (≤4.0 nm diameter semiconductor NCs) are considered to be higher than that of columbic interaction energy.[67, 68] Under this condition, wavefunctions of a photo-excited electron and/or hole could occupy the entire NC volume and leak outside of the fully inorganic perovskite core boundary. Escaped wavefunctions then entangle, resulting in electronic coupling between neighboring NCs and the formation of extended delocalization states (minibands), and thus increasing the confinement box size and cause bathochromic shifts in the lowest energy absorption peak, as reported for only metal chalcogenide quantum dots[60, 69-72,] but yet to be demonstrated for CsPbBr3 NCs. Solvent-like properties and low hydrodynamic radii of PEG should facilitate such electronic coupling. Under such circumstances, where inter-NC electronic coupling is the major contributor to observed bathochromic shifts of 3.0 nm diameter $CsPbBr_3$ NCs in various assemblies, one would expect a strong relationship between the spatial distance (NC edge-to-edge separation) and E_{op}. This is due to the fact that as the spacing increases, electronic coupling strength decreases, and therefore E_{op} increases (less influence on the E_{op}). **Figure 5A** illustrates a near linear relationship between inter-NC spacing and E_{op} for four different assemblies in which the highest reduction of optical band-gap is observed for 2D closed-packed assemblies. We are unable to determine inter-$CsPbBr_3$ NC spacing in the nanorice assembly due to their highly closely packed and overlapping spatial organization. The PL characterization also shows continuous red-shifting in the peak position from lamellar to nanorice assembly (see **Figure 4E-H).** However, these shifts can be related to a variable degree of surface defects. Unless the NCs are completely defect free, it is highly qualitative to determine the electronic coupling from the PL analysis. It is also important to mention that the dipole-dipole interaction between NCs[73, 74] and changes in the local refractive index[75-77] of NCs have the potential to induce bathochromic shifts. However, we used exactly identical chain lengths of PEG_6-NH_2 and PEG_6-COOH as ligands, therefore refractive index-related E_{op} modulation can be neglected. It is important to mention that our observed exciton wavefunction delocalization of $CsPbBr_3$ NCs in pearl necklace assemblies is a further example of a previously reported phenomenon, as polymer-functionalized gold nanoparticles organized into one-dimensional networks also show increased delocalization of excitons.[78] Taken together, the pearl necklace assembly of $CsPbBr_3$ NCs organized in one-dimensional chains having the ability to delocalize excitonic wavefunctions and provide efficient charge separation should allow long distance charge transport, and thus potentially aid fabrication of advanced optoelectronic devices.

We calculated the vdW interaction strength (V_{vdW}) between two spherical NCs (considered as hard balls) as described in literature, without considering the ligand effects in the calculation.[79, 80] Our calculations show a nearly three-fold difference in V_{vdW} between closed-packed and lamellar assemblies (**Figure 5B**). Although V_{vdW} between $CsPbBr_3$ NCs in chloroform dispersion is low but it is an attractive one. As mentioned earlier, dipole-dipole and charge-dipole interactions may also play a significant role in the overall mesoscale assembly processes, which result in a high coupling energy. We are able to calculate the van der Waals interaction, and analysis of dipole-dipole and charge-dipole interactions are ongoing and we hope to report them in future works.

Experiments were undertaken to characterize the spatial organization of surface passivating ligands (e.g., PEG_6-NH_2) on the surface of $CsPbBr_3$ NCs that lead to in-situ formation of pearl necklace assemblies. By using a ninhydrin-based assay (**Figure S10**)[81] and reported a molar extinction coefficient of ~1.0 x 10^4 $M^{-1}cm^{-1}$ of $CsPbBr_3$ NCs,[82] we determine that about ~0.7 PEG_6-NH_2/nm^2 are bound on 3.0 nm diameter $CsPbBr_3$ NCs. Supporting information file provides detailed experimental procedure for the ninhydrin-based assay and polymer grafting density calculations. According to the Flory model, such a low density of polymer grafting, specifically for the shorter chain length polymers (i.e., PEG_6-NH_2) leads to a "mushroom" structure in which polymers lay flat on the solid surface while wrapping the NCs.[83] This result supports our proposed meatball-spaghetti model (vide infra).

Based on the structural characterizations presented above, we propose the mesoscale assembly model as the basis for the formation of various nanoscale assemblies under our experimental conditions.[24] The mechanism underlying mesoscale assembly of individual inorganic NCs into higher order assemblies through cooperative interactions is controlled by the short-range vdW forces between surface passivating ligands, along with dipole-dipole and charge-dipole forces between NCs.[24, 84, 85] We believe vdW interactions between surface passivating ligands induce mesoscale assembly and drive adjacent $CsPbBr_3$ NCs closer together to form pearl necklace assemblies with regular inter-NC spacing (**Figure 4A**). Importantly, this assembly is only observed when PEG_6-NH_2 is present in the reaction medium. PEG_6-NH_2 is hydrophilic in nature; therefore some excess ligands are expected to be present in NCs even after purification in hydrophobic solvent (hexane/toluene mixture). Furthermore, the chloroform (a non-polar solvent) in which $CsPbBr_3$ NCs are dispersed should favor vdW interactions between PEG_6 chains. Additionally, a cubic $CsPbBr_3$ crystal has an inherent dipole moment,[86] that would assist dipole-dipole interactions between NCs. The hydrodynamic radii of PEG_6 in solution is 0.6 nm and it forms coil structures.[60] The inter-$CsPbBr_3$ NC spacing in an individual pearl-necklace assembly is 2.4 nm, which is ~1.0 nm larger than twice the hydrodynamic radii of PEG_6. This may also suggest the presence of excess PEG_6 between NCs, possibly as interdigitated structures leading to vdW interactions, which readily facilitate the thermodynamically controlled mesoscale assembly of NCs into higher order superstructures. As shown in **Figure S6B**, pearl-necklace assemblies are present in a long-range linear array. This is only possible because of the size monodispersity of NCs that helps crystal-face specific interactions between the hydrophilic tails of surface-bound PEG_6 ligands. Additionally, sufficiently high binding affinity between –NH_2 and surface Br^- of $CsPbBr_3$ NC, along with dative interactions between Pb^{2+} and glycol units (-CH_2-CH_2-O-) of PEG_6 provide high stability of NCs. This results in no further crystal growth within the pearl-necklace assembly, as previously observed for CdTe nanowire formation from the corresponding pearl necklace structures.[26]

The formation of bundled pearl necklace assemblies of $CsPbBr_3$ NCs, in which long pearl necklace structures retain their one-dimensional arrangement, are observed (see **Figure 4B**) when the synthesis was performed in the presence of a slightly higher concentration of PEG_6-

NH_2. Although the passivating ligand PEG_6-NH_2 is hydrophilic in nature, it is still soluble in chloroform due to a unique solubility property.[60] In this context, the solvent layer from the surface of ligand-passivated NCs is expected to be repelled by PEG_6-NH_2. Therefore, the existing cooperative interactions between individual pearl-necklace assemblies is expected to increase, pushing pearl necklace assemblies towards each other, and this result in the formation of bundled assemblies of $CsPbBr_3$ NCs.[87] Further increasing PEG_6-NH_2 concentrations in the reaction mixture produces lamellar assemblies in which $CsPbBr_3$ NCs are uniformly distributed throughout the structure (see **Figure 4C**). A continuous increase in inter-NC spacing is observed from individual necklace to bundled necklace and then to lamellar assemblies (**Figure 5**) due to presence of extra PEG_6 between NCs. When both PEG_6-NH_2 and PEG_6-COOH were used in the synthesis, nanorice assemblies are formed rather than one-dimensional assemblies of $CsPbBr_3$ NCs. This is presumably because of the strong electrostatic and hydrogen bonding interactions between –COOH and –NH_2 groups. Although these attractive forces bring the NCs closer, individual NCs are not fused together and they form aggregated structures. Soft and flexible PEG chains passivate the surface of NCs through multiple dative bonds - Pb of $CsPbBr_3$ could datively interact with the oxygen in the glycol units-similar to a meatball and spaghetti structure. Overall, solution-based self-assembly of NCs into higher order superstructures through the thermodynamically-driven mesoscale assembly process lies in the delicate interplay between the various forces discussed above, including the polarity of the solvent. Additionally, presence of excess ligands in the purified $CsPbBr_3$ NC samples plays a significant role in the mesoscale assembly process, which could be difficult to achieve through a post-synthetic ligand exchange reaction. Nevertheless, precise quantification of these interactions is beyond the scope of this article. We should mention that other parameters such as reaction temperature and the rate of solvent evaporation could also influence the mesoscale assembly process. In this work, all syntheses were performed under identical temperature and all TEM samples were prepared using the same protocol (see Supporting Information). Therefore, we believe temperature and microscopy sample preparation do not influence the formation of higher order superstructures of $CsPbBr_3$ NCs.

As described above, it is suggested that all higher order superstructures of spherical ~3.0 nm $CsPbBr_3$ NCs are driven and stabilized through various interactions of surface passivating ligands, and not by cross-linking between individual PEG_6 units. Therefore, we hypothesize that one type of assembly (e.g., pearl necklace) can be converted to other assembles (e.g., lamellar and/or nanorice) by controlling ligand interactions (e.g., vdW) through post-synthetic ligand treatment (**Figure 3**). To further examine the unique role of surface passivating ligands in the mesoscale assembly, individual pearl necklace assemblies were prepared by using 0.2 mmol of PEG_6-NH_2. Samples were treated separately with (i) 0.4 mmol of PEG_6-NH_2 and (ii) 0.2 mmol PEG_6-COOH. As shown in Figure **6A-B**, lamellar and nanorice assemblies are formed in the presence of PEG_6-NH_2 and PEG_6-COOH, respectively. These control experiments definitely support our proposed model of ligand-controlled mesoscale assembly of $CsPbBr_3$ NCs and formation of superstructures. If the entire hypothesis holds true we then expect that methyl-terminated PEG (PEG_6-CH_3) - with an identical chain length of PEG_6-NH_2 – should drive the mesoscale assembly and convert individual pearl necklace structure to either bundled pearl necklace or lamellar assemblies, as shown in **Figure S11**. Overall, these control experiments prove that the appropriate selection of surface passivating ligands in the colloidal synthesis of $CsPbBr_3$ NCs has the unique ability to participate in various interactions and promote mesoscale assembly processes in solution, thereby resulting in the formation of higher-order superstructures.

Template-Free Hierarchical Self-Assembly of $CsPbBr_3$ NCs into Superlattice Structures. It is noteworthy to mention that within nearly 24 h, the storage of individual pearl necklace assemblies of $CsPbBr_3$ NCs in chloroform dispersion produce hierarchical, twisted ribbon structures (**Figure 6C**), similar to CdTe/CdS structures reported in the literature.[88] The ribbons are extended to micron length forming superlattice structures. A closer look (**Figure S12**) reveals the presence of individual necklaces at the ribbon's top. The formation of higher order superstructures can also be observed for nanorice assemblies in which individual rice is connected to form chain-like structures (**Figure 6D**). The hierarchical superstructure formation can be monitored visually by the appearance of turbidity in the originally clear solution of $CsPbBr_3$ NCs. We do not fully understand what parameters drive the hierarchical superstructure formation, but we speculate that PEG_6- PEG_6 (NC surface bound and/or free unbound) interactions within the hydrophobic solvent of the template-free process may play a significant role. Nevertheless, a more detailed investigation, possibly including time-dependent microscopic characterization, may unravel the mechanism underlying the hierarchical superstructure formation; this represents ongoing research within our laboratory.

CONCLUSIONS

In summary, we have demonstrated a facile colloidal synthetic method for the preparation of flexible polymer-passivated, nearly monodispersed $CsPbBr_3$ NCs. Depending on the concentration and binding head group of the surface passivating ligand PEG_6-NH_2/COOH, various self-assembled structures of NCs such as individual and bundled pearl-necklaces, lamellar, nanorice are formed in-situ. In the thermodynamically controlled mesoscale assembly process, vdW interactions between polymeric passivating ligands and dipole-dipole interactions of NCs contribute substantially to the formation of these uniquely organized assemblies. Although, we have studied the effects of concentration and binding head group of the surface passivating ligand on the assembly formation, one would expect that the chain length of PEG ligands should produce different structures because of the variable degree of cooperative interactions. As a proof-of-concept, we conducted the synthesis using additionally three different chain lengths PEG_n-NH_2 (n = 4, 12, and 18). We have observed the formation of nanowires for PEG_4-NH_2, and pearl necklaces and micro-size nanosheets containing individual spherical NCs for PEG_{12}-NH_2 and PEG_{18}-NH_2, respectively (data not shown). Importantly, strong electronic coupling between NCs, due to delocalization and entanglement of excitonic wavefunctions in the close-packed assembly has resulted in significant alteration of optical band-gaps and the higher-order hybrid nanostructures obtained behave more like artificial solids. Finally, both pearl-necklace and/or nanorice assembly form hierarchical superstructures that can be further refined to produce complex and unique self-assembled structures that mimic those found in the nature. Taken together, our work on polymer-assisted synthesis of higher order superstructures of $CsPbBr_3$ NCs consisting of regular ordering and with strong inter-NC electronic coupling leading to collective optoelectronic properties, along with the reported facile charge transport abilities of PEGs[89, 90] may enhance the efficiency of photovoltaic and light emitting devices.[7-11]

EXPERIMENTAL SECTION

Chemicals. Poly(ethylene glycol) methyl ethers (PEG_6-OH), *p*-toluene sulfonyl chloride (>99%), lead bromide ($PbBr_2$, >99%), potassium phthalimide (98%), cesium carbonate (99.9%), hydrazine monohydrate (98%), succinc anhydride, 4-(dimethylamino)pyrindine, triethyl amine, 1,4 dioxane, carbon tetrachloride (99.9%), 1-octadecene (90% technical grade), anhydrous acetonitrile (CH_3CN, >99.8%), toluene (99.9%) hexane (99%), ethanol (98.5%), chloroform (>99%), and dichloromethane (DCM, >99%) were purchased from Aldrich and used without further purification. Different chain length PEG_n-amines (n = 4, 12, and 18) were purchased from Biochempeg, MA. Tetrahydrofuran (99.9%), sodium hydroxide, sodium sulphate anhydrous, and methanol (99.9%) were purchased from Fisher and used without further purification. Organic solvents were purged with N_2 for 30 min prior to use.

Synthesis of Cesium Lead Bromide Perovskite Nanocrystals. In a 25 mL round bottom flask, 3.0 mL ODE along with desired amount of PEG_6-amine (60-120 μL) and PEG_6-acid (0-20 μL) were mixed together and then the reaction mixture was heated at 65° C for 45 min under stirring. Separately, 5.0 mg of PEG_6-COO-Cs was placed in a small vial and dispersed in ODE (200 μL) by sonication then injected into the round bottom flask, and the reaction mixture was stirred for an additional 30 min. Next, 25.0 mg $PbBr_2$ was dissolved in 200 μL DMSO and injected into the flask and allowed to react for 15 sec. At this point, the reaction mixture was injected into 5.0 mL hexane and toluene mixture (7:3 volume ratio) to quench the reaction. The product was isolated through centrifugation at 5000 rpm for 5 min, and the resulting product was then redissolved in chloroform and centrifuged again at 5000 rpm for 5 min to remove any insoluble materials. The yellow supernatant was collected for spectroscopy and microscopy analyses.

UV-vis Absorbance, Photoluminescence, and NMR Analyses. The absorption spectra were collected using a Varian-Cary 50 Scan UV-visible spectrophotometer with 1 cm quartz cuvettes over a range of 300-800 nm. All spectra were recorded in chloroform, and chloroform was used as a background for all measurements. The photoluminescence emission (PL) spectra were collected using a Cary Eclipse fluorescence spectrophotometer from Varian Instruments with 1 cm quartz cuvettes. H^1 NMR spectra were recorded on a Bruker Avance III 500 instrument at 500 MHz frequency using $CDCl_3$ as solvent.

Elemental Analysis. A field emission scanning electron microscopy system (Hitachi S-4700), which was equipped with an energy dispersive X-ray (EDS) analyzer, was used to determine the Cs:Pb:Br ratio.

Powder X-ray Diffraction (PXRD) Analysis. Wide-angle PXRD was recorded on a Rigaku MiniFlexTM II (Cu Kα) instrument. Samples were prepared by drop-casting the purified perovskite nanocrystals on cleaned glass coverslips. All samples were run from 10°- 60° with 0.015° increments at 1.5 s per step.

Transmission Electron Microscopy (TEM) Characterization. The samples for TEM analysis were prepared by placing 10 μL of the sample dissolved in chloroform onto a carbon-coated copper grid (Electron Microscopy Science). The sample was allowed to set for 30 seconds and any excess solution was removed by wicking with a Kimwipe in order to avoid particle aggregation. Images were acquired using a JEOL-3200FS-JEM instrument operating at 200 kV. At least 300 NCs were analyzed for diameter averaging. At least 100 inter-NC spacing were used to determine average and standard deviation.

ASSOCIATED CONTENT

Supporting Information. Detailed experimental procedures for ligands synthesis, various spectroscopy and microscopy characterizations, histograms for size and dimension analyses, and additional micrographs. These materials are available free of charge. (PDF)

AUTHOR INFORMATION

Corresponding Author

*Rajesh Sardar; Email: rsardar@iupui.edu

Author Contributions

[$]These authors contributed equally to this work.

ACKNOWLEDGMENT

The authors acknowledge financial support by the National Science Foundation under grant no. NSF DMR-1747582. The authors thank Dr. D. Minner (IUPUI) for helpful discussions.

Figures and Table

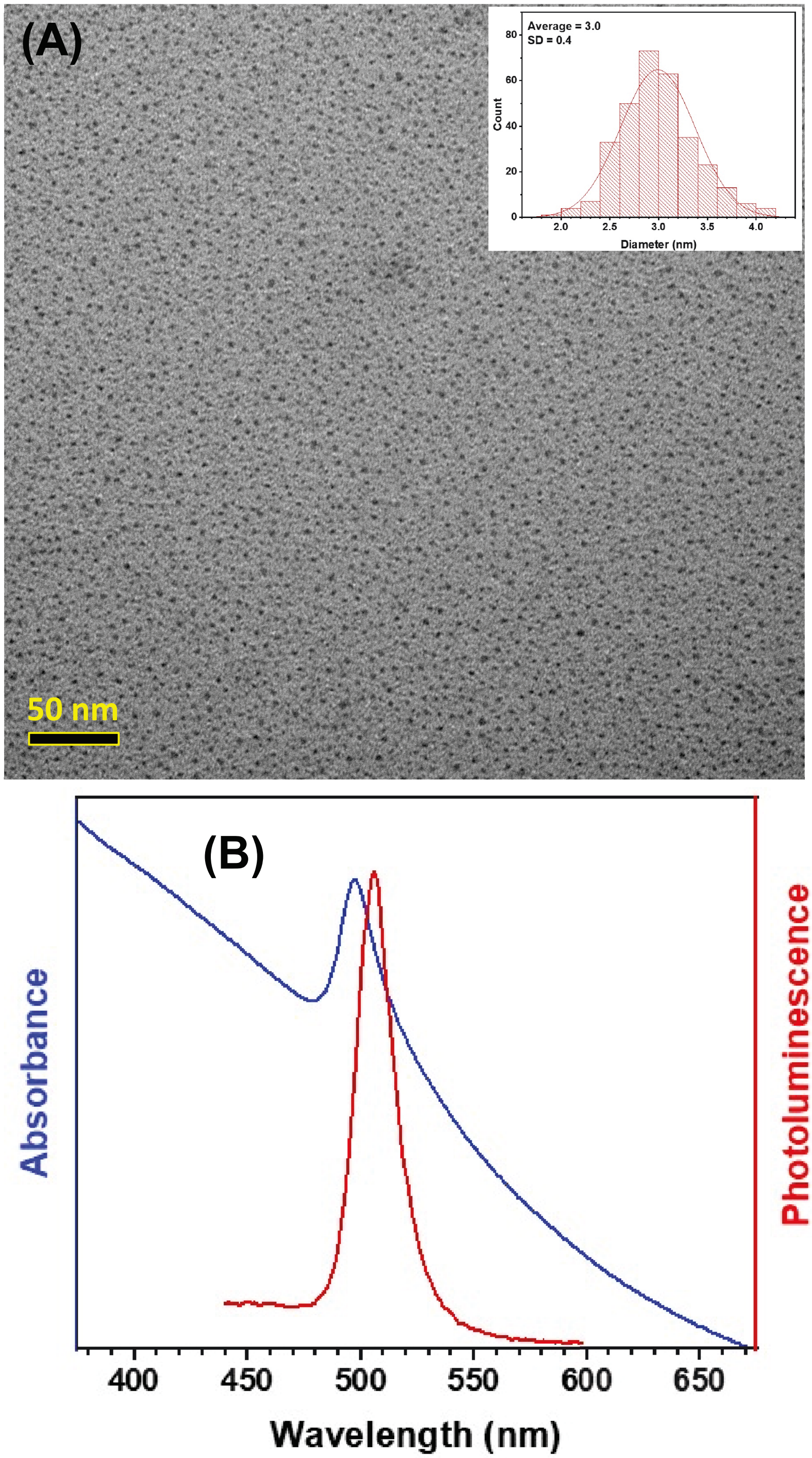

Figure 1. (A) Low-magnification TEM image of $CsPbBr_3$ NCs synthesized using 10 and 60 μL of PEG_6-COOH and PEG_6-NH_2, respectively. The inset shows a histogram of size analysis. Approximately 300 NCs were counted to determine the average and standard deviation. (B) UV-

visible absorption (blue line) and photoluminescence (red line) spectra of average 3.1 nm diameter $CsPbBr_3$ NCs. The photoluminescence spectrum was collected at 380 nm excitation wavelength.

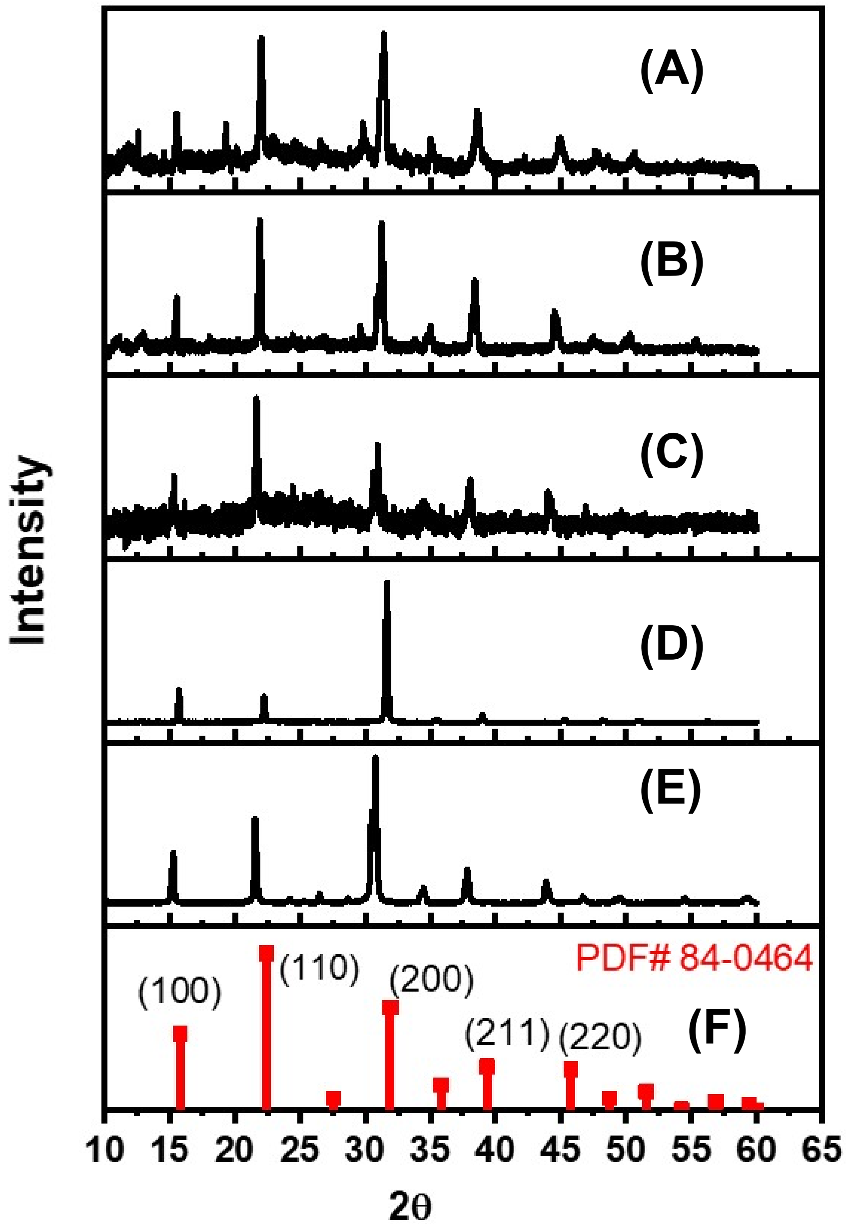

Figure 2. XRD pattern of $CsPbBr_3$ NCs synthesized in the presence of different amount of PEG_6-COOH and PEG_6-NH_2: (A) close-packed, (B) individual pearl necklace, (C) bundled pearl necklace, (D) lamellar, (E) nanorice assemblies and (F) standard XRD pattern.

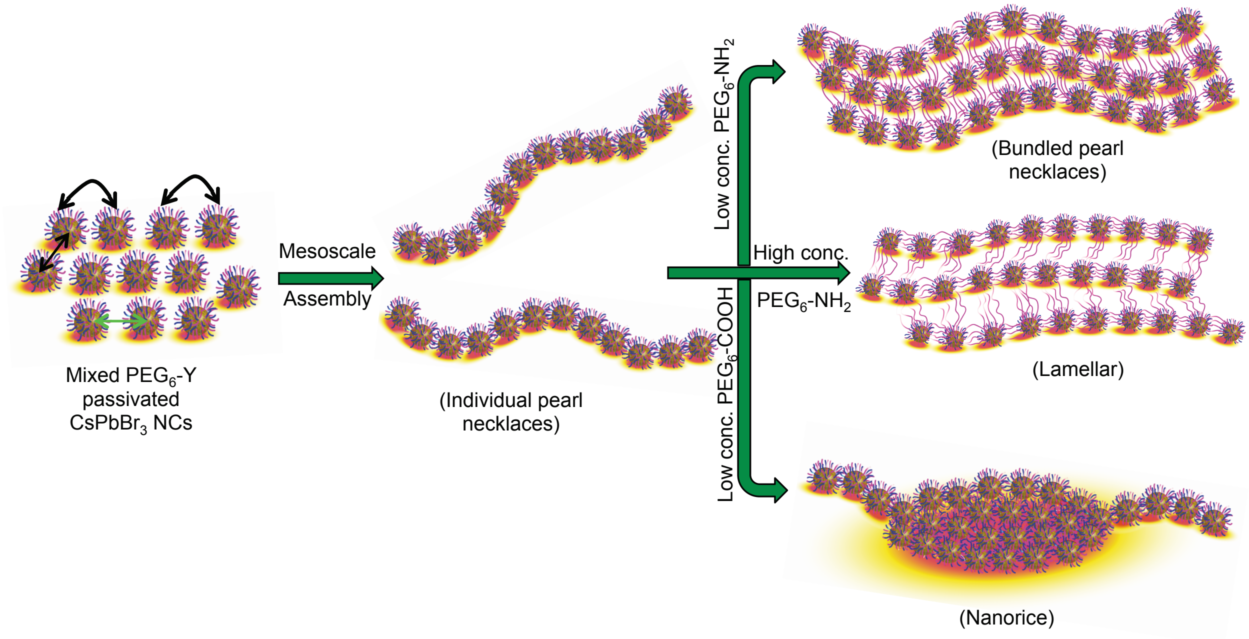

Figure 3. Schematic representation of ligand-assisted mesoscale transformations and formation of higher-order hybrid nanostructures (superstructures). Van der Waals interactions between hydrophilic PEG tails (double-headed black arrows) in a nonpolar solvent, and dipole-dipole attraction between NCs (double-headed green arrows) drive the mesoscale assembly to form superstructures. In the hairy-ball model, blue and purple curves represent PEG_6-COOH and PEG_6-NH_2, respectively. Long-range cooperative interactions between superstructures produce hierarchical superstructures with micron length scale.

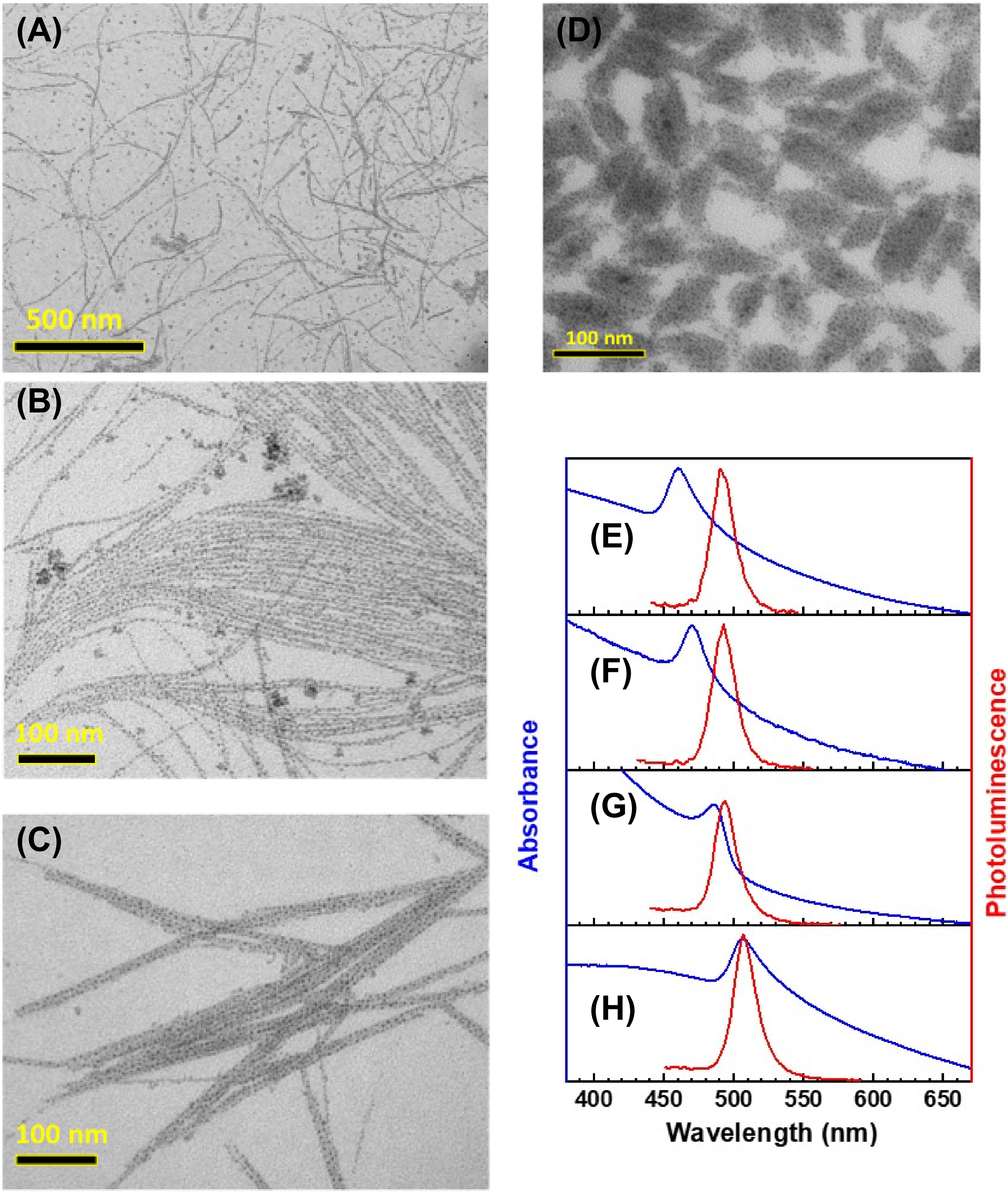

Figure 4. TEM micrographs of pearl-necklace (A), bundled (B), lamellar (C), and nanorice (D) assemblies of $CsPbBr_3$ NCs synthesized in the presence of different amount of PEG_6-NH_2 (A-C)

but no PEG_6-COOH, and using both PEG_6-COOH and PEG_6-NH_2 (D). UV-visible absorption (blue lines) and photoluminescence (red lines) spectra of lamellar (E), bundled (F), pearl-necklace (G), and nanorice (H) assemblies of $CsPbBr_3$ NCs.

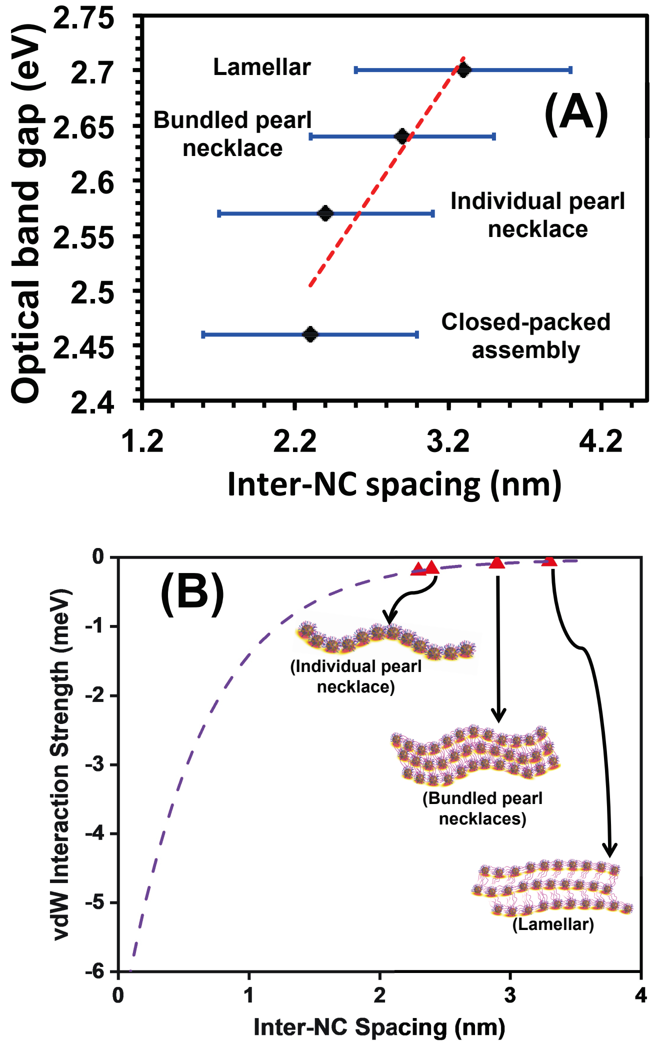

Figure 5. (A) Relationship depicting experimentally determined optical band-gap of $CsPbBr_3$ NCs as a function of inter-NC spacing. The size of the NCs is ~3.0 nm. Dotted red line shows a linear correlation (R2 = 0.956). According to effective mass approximation calculations, the band-gap of 3.0 nm diameter $CsPbBr_3$ NCs is expected to be 4.46 eV.[12, 63] Bulk band-gap of $CsPbBr_3$ perovskite is 2.25 eV.[64] (B) The red triangles are from a theoretical calculation of V_{vdW} between two adjacent NCs. Insets are the corresponding images of the self-assembly superstructure. Blue dash line illustrates the trend of the change of V_{vdW} with respect to the inter-NC spacing. The dash line represents nonlinear curve fitting based on the calculations.

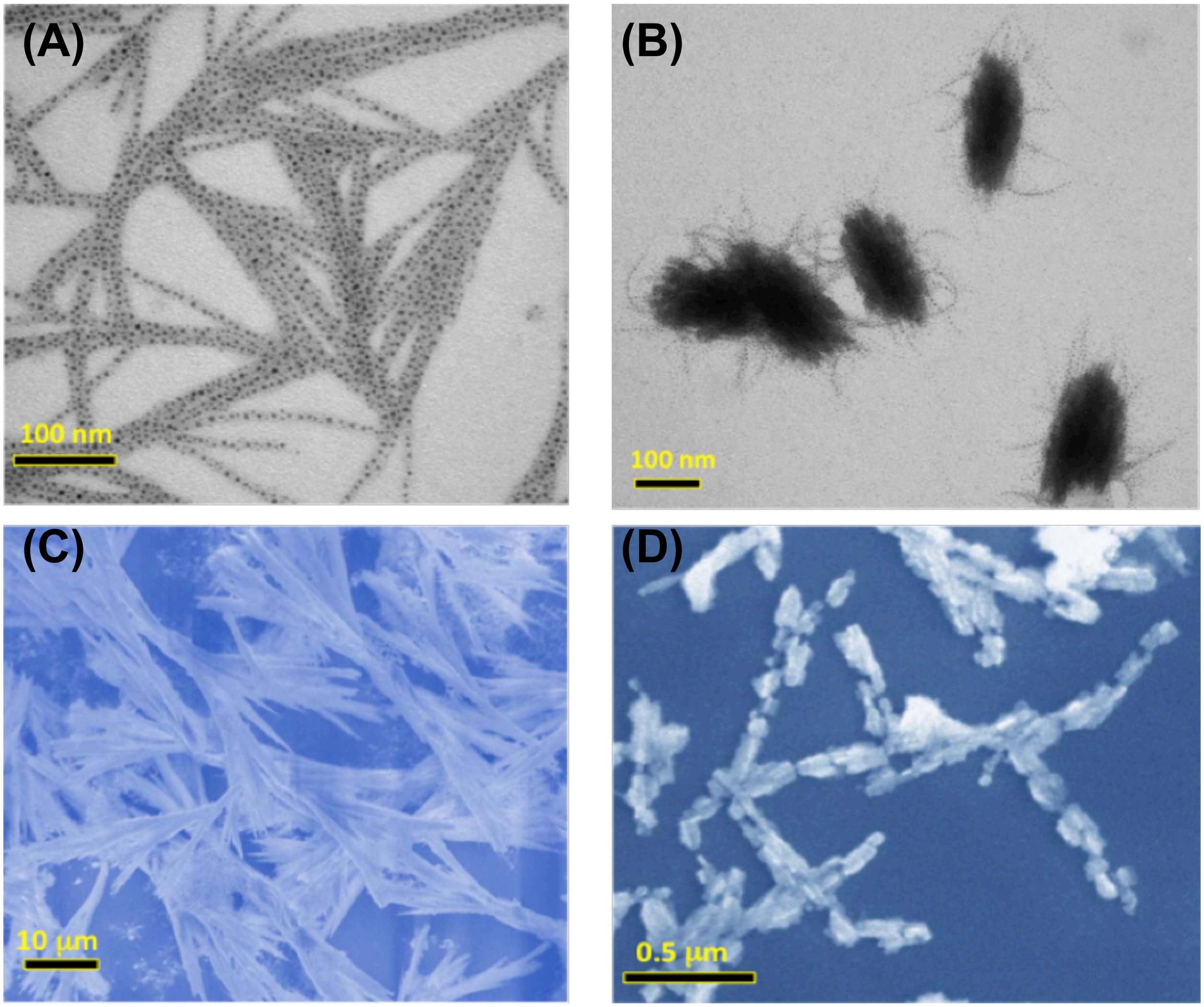

Figure 6. Representative TEM images showing lamellar **(A)** and nanorice **(B)** assemblies of $CsPbBr_3$ NCs prepared from pearl-necklace assemblies by adding 0.2 mmol PEG_6-NH_2 (A) 0.06 mmol and PEG_6-COOH (B) at room temperature. SEM micrographs of twisted ribbons **(C)** and inter-connected nanorices **(D)** of $CsPbBr_3$ NCs.

Table 1. Comparison of absorption, Photoluminescence, Size, and Inter-NC Spacing of $CsPbBr_3$ NCs in Various Assemblies, Which Were Prepared Using PEG_6-NH_2 and/or PEG_6-COOH of Different Concentrations.

reagent concentration	UV-visible absorption peak position, nm (eV)	PL peak position, nm (eV)	NC diameter (nm)	inter–NC spacing (nm)	length (nm)	NC assembly
0.4 mmol PEG_6-NH_2 and no PEG_6-COOH	460 (2.70)	490 (2.53)	3.0 ± 0.5	3.3 ± 0.7	N/A	lamellar
0.34 mmol PEG_6-NH_2 and no PEG_6-COOH	470 (2.64)	493 (2.52)	3.0 ± 0.5	2.9 ± 0.6	584 ± 150	bundled pearl-necklace
0.2 mmol PEG_6-NH_2 and no PEG_6-COOH	483 (2.57)	495 (2.51)	3.0 ± 0.4	2.4 ± 0.7	533 ± 133	individual pearl-necklace
0.03 mmol PEG_6-COOH and 0.2 mmol PEG_6-NH_2	494 (2.51)	504 (2.46)	3.0 ± 0.4	2.3 ± 0.7	N/A	closed-packed self-assembly
0.06 mmol PEG_6-COOH and 0.2 mmol PEG_6-NH_2	505 (2.46)	508 (2.44)	3.1 ± 0.5	N/A	N/A	nanorice

REFERENCES

1. Zhang, Q.; Yin, Y. All-Inorganic Metal Halide Perovskite Nanocrystals: Opportunities and Challenges. *ACS Central Sci.* **2018**, *4*, 668-679.
2. Akkerman, Q. A.; Rainò, G.; Kovalenko, M. V.; Manna, L. Genesis, challenges and opportunities for colloidal lead halide perovskite nanocrystals. *Nat. Mater.* **2018**, *17*, 394-405.
3. Becker, M. A.; Vaxenburg, R.; Nedelcu, G.; Sercel, P. C.; Shabaev, A.; Mehl, M. J.; Michopoulos, J. G.; Lambrakos, S. G.; Bernstein, N.; Lyons, J. L.*, et al.* Bright triplet excitons in caesium lead halide perovskites. *Nature* **2018**, *553*, 189.
4. Wu, K.; Liang, G.; Shang, Q.; Ren, Y.; Kong, D.; Lian, T. Ultrafast Interfacial Electron and Hole Transfer from CsPbBr3 Perovskite Quantum Dots. *J. Am. Chem. Soc.* **2015**, *137*, 12792-12795.
5. Brumberg, A.; Diroll, B. T.; Nedelcu, G.; Sykes, M. E.; Liu, Y.; Harvey, S. M.; Wasielewski, M. R.; Kovalenko, M. V.; Schaller, R. D. Material Dimensionality Effects on Electron Transfer Rates Between CsPbBr3 and CdSe Nanoparticles. *Nano Lett.* **2018**, *18*, 4771-4776.
6. Sarkar, S.; Ravi, V. K.; Banerjee, S.; Yettapu, G. R.; Markad, G. B.; Nag, A.; Mandal, P. Terahertz Spectroscopic Probe of Hot Electron and Hole Transfer from Colloidal CsPbBr3 Perovskite Nanocrystals. *Nano Lett.* **2017**, *17*, 5402-5407.
7. Zai, H.; Zhu, C.; Xie, H.; Zhao, Y.; Shi, C.; Chen, Z.; Ke, X.; Sui, M.; Chen, C.; Hu, J.*, et al.* Congeneric Incorporation of CsPbBr3 Nanocrystals in a Hybrid Perovskite Heterojunction for Photovoltaic Efficiency Enhancement. *ACS Energy Lett.* **2018**, *3*, 30-38.
8. Li, G.; Wang, H.; Zhang, T.; Mi, L.; Zhang, Y.; Zhang, Z.; Zhang, W.; Jiang, Y. Solvent-Polarity-Engineered Controllable Synthesis of Highly Fluorescent Cesium Lead Halide Perovskite Quantum Dots and Their Use in White Light-Emitting Diodes. *Adv. Func. Mater.* **2016**, *26*, 8478-8486.
9. Song, J.; Li, J.; Xu, L.; Li, J.; Zhang, F.; Han, B.; Shan, Q.; Zeng, H. Room-Temperature Triple-Ligand Surface Engineering Synergistically Boosts Ink Stability, Recombination Dynamics, and Charge Injection toward EQE-11.6% Perovskite QLEDs. *Adv. Mater.* **2018**, *30*, 1800764-7.
10. Yakunin, S.; Protesescu, L.; Krieg, F.; Bodnarchuk, M. I.; Nedelcu, G.; Humer, M.; De Luca, G.; Fiebig, M.; Heiss, W.; Kovalenko, M. V. Low-threshold amplified spontaneous emission and lasing from colloidal nanocrystals of caesium lead halide perovskites. *Nat. Commun.* **2015**, *6*, 8056-8064.
11. Sanehira, E. M.; Marshall, A. R.; Christians, J. A.; Harvey, S. P.; Ciesielski, P. N.; Wheeler, L. M.; Schulz, P.; Lin, L. Y.; Beard, M. C.; Luther, J. M. Enhanced mobility CsPbI₃ quantum dot arrays for record-efficiency, high-voltage photovoltaic cells. *Sci. Adv.* **2017**, *3*.
12. Protesescu, L.; Yakunin, S.; Bodnarchuk, M. I.; Krieg, F.; Caputo, R.; Hendon, C. H.; Yang, R. X.; Walsh, A.; Kovalenko, M. V. Nanocrystals of Cesium Lead Halide Perovskites (CsPbX3, X = Cl, Br, and I): Novel Optoelectronic Materials Showing Bright Emission with Wide Color Gamut. *Nano Lett.* **2015**, *15*, 3692-3696.

13. Pan, A.; He, B.; Fan, X.; Liu, Z.; Urban, J. J.; Alivisatos, A. P.; He, L.; Liu, Y. Insight into the Ligand-Mediated Synthesis of Colloidal CsPbBr3 Perovskite Nanocrystals: The Role of Organic Acid, Base, and Cesium Precursors. *ACS Nano* **2016**, *10*, 7943-7954.
14. Swarnkar, A.; Chulliyil, R.; Ravi, V. K.; Irfanullah, M.; Chowdhury, A.; Nag, A. Colloidal CsPbBr3 Perovskite Nanocrystals: Luminescence beyond Traditional Quantum Dots. *Angew. Chem. Inter. Ed.* **2015**, *54*, 15424-15428.
15. Tong, Y.; Bohn, B. J.; Bladt, E.; Wang, K.; Müller-Buschbaum, P.; Bals, S.; Urban, A. S.; Polavarapu, L.; Feldmann, J. From Precursor Powders to CsPbX3 Perovskite Nanowires: One-Pot Synthesis, Growth Mechanism, and Oriented Self-Assembly. *Angew. Chem. Inter. Ed.* **2017**, *56*, 13887-13892.
16. Imran, M.; Di Stasio, F.; Dang, Z.; Canale, C.; Khan, A. H.; Shamsi, J.; Brescia, R.; Prato, M.; Manna, L. Colloidal Synthesis of Strongly Fluorescent CsPbBr3 Nanowires with Width Tunable down to the Quantum Confinement Regime. *Chem. Mater.* **2016**, *28*, 6450-6454.
17. Akkerman, Q. A.; D'Innocenzo, V.; Accornero, S.; Scarpellini, A.; Petrozza, A.; Prato, M.; Manna, L. Tuning the Optical Properties of Cesium Lead Halide Perovskite Nanocrystals by Anion Exchange Reactions. *J. Am. Chem. Soc.* **2015**, *137*, 10276-10281.
18. Akkerman, Q. A.; Motti, S. G.; Srimath Kandada, A. R.; Mosconi, E.; D'Innocenzo, V.; Bertoni, G.; Marras, S.; Kamino, B. A.; Miranda, L.; De Angelis, F.*, et al.* Solution Synthesis Approach to Colloidal Cesium Lead Halide Perovskite Nanoplatelets with Monolayer-Level Thickness Control. *J. Am. Chem. Soc.* **2016**, *138*, 1010-1016.
19. Bekenstein, Y.; Koscher, B. A.; Eaton, S. W.; Yang, P.; Alivisatos, A. P. Highly Luminescent Colloidal Nanoplates of Perovskite Cesium Lead Halide and Their Oriented Assemblies. *J. Am. Chem. Soc.* **2015**, *137*, 16008-16011.
20. Shamsi, J.; Dang, Z.; Bianchini, P.; Canale, C.; Stasio, F. D.; Brescia, R.; Prato, M.; Manna, L. Colloidal Synthesis of Quantum Confined Single Crystal CsPbBr3 Nanosheets with Lateral Size Control up to the Micrometer Range. *J. Am. Chem. Soc.* **2016**, *138*, 7240–7243.
21. Zhang, D.; Eaton, S. W.; Yu, Y.; Dou, L.; Yang, P. Solution-Phase Synthesis of Cesium Lead Halide Perovskite Nanowires. *J. Am. Chem. Soc.* **2015**, *137*, 9230-9233.
22. Aharon, S.; Etgar, L. Two Dimensional Organometal Halide Perovskite Nanorods with Tunable Optical Properties. *Nano Lett.* **2016**, *16*, 3230-3235.
23. Nedelcu, G.; Protesescu, L.; Yakunin, S.; Bodnarchuk, M. I.; Grotevent, M. J.; Kovalenko, M. V. Fast Anion-Exchange in Highly Luminescent Nanocrystals of Cesium Lead Halide Perovskites (CsPbX3, X = Cl, Br, I). *Nano Lett.* **2015**, *15*, 5635-5640.
24. Cölfen, H.; Mann, S. Higher-Order Organization by Mesoscale Self-Assembly and Transformation of Hybrid Nanostructures. *Angew. Chem. Int. Ed.* **2003**, *42*, 2350-2365.
25. Miszta, K.; de Graaf, J.; Bertoni, G.; Dorfs, D.; Brescia, R.; Marras, S.; Ceseracciu, L.; Cingolani, R.; van Roij, R.; Dijkstra, M.*, et al.* Hierarchical self-assembly of suspended branched colloidal nanocrystals into superlattice structures. *Nature Mater.* **2011**, *10*, 872-876.
26. Tang, Z.; Kotov, N. A.; Giersig, M. Spontaneous Organization of Single CdTe Nanoparticles into Luminescent Nanowires. *Science* **2002**, *297*, 237-240.

27. Tang, Z.; Zhang, Z.; Wang, Y.; Glotzer, S. C.; Kotov, N. A. Self-Assembly of CdTe Nanocrystals into Free-Floating Sheets. *Science* **2006**, *314*, 274-278.
28. Teunis, M. B.; Jana, A.; Dutta, P.; Johnson, M. A.; Mandal, M.; Muhoberac, B. B.; Sardar, R. Mesoscale Growth and Assembly of Bright Luminescent Organolead Halide Perovskite Quantum Wires. *Chem. Mater.* **2016**, *28*, 5043-5054.
29. Teunis, M. B.; Johnson, M. A.; Muhoberac, B. B.; Seifert, S.; Sardar, R. Programmable Colloidal Approach to Hierarchical Structures of Methylammonium Lead Bromide Perovskite Nanocrystals with Bright Photoluminescent Properties. *Chem. Mater.* **2017**, *29*, 3526-3537.
30. Nakata, K.; Hu, Y.; Uzun, O.; Bakr, O.; Stellacci, F. Chains of Superparamagnetic Nanoparticles. *Adv. Mater.* **2008**, *20*, 4294-4299.
31. Deng, Z.; Tian, Y.; Lee, S.-H.; Ribbe, A. E.; Mao, C. DNA-Encoded Self-Assembly of Gold Nanoparticles into One-Dimensional Arrays. *Angew. Chem. Inter. Ed.* **2005**, *44*, 3582-3585.
32. Marinakos, S. M.; Brousseau, L. C.; Jones, A.; Feldheim, D. L. Template Synthesis of One-Dimensional Au, Au−Poly(pyrrole), and Poly(pyrrole) Nanoparticle Arrays. *Chem. Mater.* **1998**, *10*, 1214-1219.
33. Korth, B. D.; Keng, P.; Shim, I.; Bowles, S. E.; Tang, C.; Kowalewski, T.; Nebesny, K. W.; Pyun, J. Polymer-Coated Ferromagnetic Colloids from Well-Defined Macromolecular Surfactants and Assembly into Nanoparticle Chains. *J. Am. Chem. Soc.* **2006**, *128*, 6562-6563.
34. Sardar, R.; Shumaker-Parry, J. S. Asymmetrically Functionalized Gold Nanoparticles Organized in One-Dimensional Chains. *Nano Lett.* **2008**, *8*, 731-736.
35. Wyrwa, D.; Beyer, N.; Schmid, G. One-Dimensional Arrangements of Metal Nanoclusters. *Nano Lett.* **2002**, *2*, 419-421.
36. Warner, M. G.; Hutchison, J. E. Linear assemblies of nanoparticles electrostatically organized on DNA scaffolds. *Nat. Mater.* **2003**, *2*, 272-277.
37. DeVries, G. A.; Brunnbauer, M.; Hu, Y.; Jackson, A. M.; Long, B.; Neltner, B. T.; Uzun, O.; Wunsch, B. H.; Stellacci, F. Divalent Metal Nanoparticles. *Science* **2007**, *315*, 358-361.
38. Guo, Y.; Harirchian-Saei, S.; Izumi, C. M. S.; Moffitt, M. G. Block Copolymer Mimetic Self-Assembly of Inorganic Nanoparticles. *ACS Nano* **2011**, *5*, 3309-3318.
39. Shah, P. S.; Sigman, M. B.; Stowell, C. A.; Lim, K. T.; Johnston, K. P.; Korgel, B. A. Single-Step Self-Organization of Ordered Macroporous Nanocrystal Thin Films. *Adv. Mater.* **2003**, *15*, 971-974.
40. Böker, A.; Lin, Y.; Chiapperini, K.; Horowitz, R.; Thompson, M.; Carreon, V.; Xu, T.; Abetz, C.; Skaff, H.; Dinsmore, A. D.*, et al.* Hierarchical nanoparticle assemblies formed by decorating breath figures. *Nat. Mater.* **2004**, *3*, 302-306.
41. Li, M.; Schnablegger, H.; Mann, S. Coupled synthesis and self-assembly of nanoparticles to give structures with controlled organization. *Nature* **1999**, *402*, 393-395.
42. Lin, Y.; Böker, A.; He, J.; Sill, K.; Xiang, H.; Abetz, C.; Li, X.; Wang, J.; Emrick, T.; Long, S.*, et al.* Self-directed self-assembly of nanoparticle/copolymer mixtures. *Nature* **2005**, *434*, 55-59.

43. Pal, J.; Manna, S.; Mondal, A.; Das, S.; Adarsh, K. V.; Nag, A. Colloidal Synthesis and Photophysics of M3Sb2I9 (M=Cs and Rb) Nanocrystals: Lead-Free Perovskites. *Angew. Chem. Inter. Ed.* **2017**, *56*, 14187-14191.
44. Wang, A.; Guo, Y.; Muhammad, F.; Deng, Z. Controlled Synthesis of Lead-Free Cesium Tin Halide Perovskite Cubic Nanocages with High Stability. *Chem. Mater.* **2017**, *29*, 6493-6501.
45. Zhang, Y.; Yin, J.; Parida, M. R.; Ahmed, G. H.; Pan, J.; Bakr, O. M.; Brédas, J.-L.; Mohammed, O. F. Direct-Indirect Nature of the Bandgap in Lead-Free Perovskite Nanocrystals. *J. Phys. Chem. Lett.* **2017**, *8*, 3173-3177.
46. Bekenstein, Y.; Dahl, J. C.; Huang, J.; Osowiecki, W. T.; Swabeck, J. K.; Chan, E. M.; Yang, P.; Alivisatos, A. P. The Making and Breaking of Lead-Free Double Perovskite Nanocrystals of Cesium Silver–Bismuth Halide Compositions. *Nano Lett.* **2018**, *18*, 3502-3508.
47. Shevchenko, E. V.; Talapin, D. V.; Kotov, N. A.; O'Brien, S.; Murray, C. B. Structural diversity in binary nanoparticle superlattices. *Nature* **2006**, *439*, 55-59.
48. Tang, J.; Kemp, K. W.; Hoogland, S.; Jeong, K. S.; Liu, H.; Levina, L.; Furukawa, M.; Wang, X.; Debnath, R.; Cha, D., *et al.* Colloidal-quantum-dot photovoltaics using atomic-ligand passivation. *Nature Mater.* **2011**, *10*, 765-771.
49. Talapin, D. V.; Murray, C. B. PbSe Nanocrystal Solids for n- and p-Channel Thin Film Field-Effect Transistors. *Science* **2005**, *310*, 86-89.
50. De Roo, J.; Ibáñez, M.; Geiregat, P.; Nedelcu, G.; Walravens, W.; Maes, J.; Martins, J. C.; Van Driessche, I.; Kovalenko, M. V.; Hens, Z. Highly Dynamic Ligand Binding and Light Absorption Coefficient of Cesium Lead Bromide Perovskite Nanocrystals. *ACS Nano* **2016**, *10*, 2071-2081.
51. Teunis, M. B.; Lawrence, K. N.; Dutta, P.; Siegel, A. P.; Sardar, R. Pure white-light emitting ultrasmall organic-inorganic hybrid perovskite nanoclusters. *Nanoscale* **2016**, *8*, 17433-17439.
52. Chauhan, B. P. S.; Sardar, R. Self-Assembled Stable Silver Nanoclusters and Nanonecklace Formation: Poly(methylhydrosiloxane)-Mediated One-Pot Route to Organosols. *Macromolecules* **2004**, *37*, 5136-5139.
53. Sardar, R.; Bjorge, N. S.; Shumaker-Parry, J. S. pH-Controlled Assemblies of Polymeric Amine-Stabilized Gold Nanoparticles. *Macromolecules* **2008**, *41*, 4347-4352.
54. Balazs, A. C.; Emrick, T.; Russell, T. P. Nanoparticle Polymer Composites: Where Two Small Worlds Meet. *Science* **2006**, *314*, 1107-1110.
55. Zalipsky, S. Functionalized Poly(ethylene glycols) for Preparation of Biologically Relevant Conjugates. *Bioconjugate Chem.* **1995**, *6*, 150-165.
56. Harris, J. M. LABORATORY SYNTHESIS OF POLYETHYLENE GLYCOL DERIVATIVES. *J. Macromole. Sci. Part C* **1985**, *25*, 325-373.
57. Lawrence, K. N.; Dutta, P.; Nagaraju, M.; Teunis, M. B.; Muhoberac, B. B.; Sardar, R. Dual Role of Electron-Accepting Metal-Carboxylate Ligands: Reversible Expansion of Exciton Delocalization and Passivation of Nonradiative Trap-States in Molecule-like CdSe Nanocrystals. *J. Am. Chem. Soc.* **2016**, *138*, 12813-12825.
58. Zhou, Y.; Wang, F.; Buhro, W. E. Large Exciton Energy Shifts by Reversible Surface Exchange in 2D II–VI Nanocrystals. *J. Am. Chem. Soc.* **2015**, *137*, 15198-15208.
59. Jasieniak, J.; Califano, M.; Watkins, S. E. Size-Dependent Valence and Conduction Band-Edge Energies of Semiconductor Nanocrystals. *ACS Nano* **2011**, *5*, 5888-5902.

60. Lawrence, K. N.; Johnson, M. A.; Dolai, S.; Kumbhar, A.; Sardar, R. Solvent-like ligand-coated ultrasmall cadmium selenide nanocrystals: strong electronic coupling in a self-organized assembly. *Nanoscale* **2015**, *7*, 11667-11677.
61. Sudeep, P. K.; Emrick, T. Pearls of Wisdom: Stringing Nanoparticles and Polymers into New Assemblies and Materials. *ACS Nano* **2009**, *3*, 2870-2875.
62. Wheeler, L. M.; Sanehira, E. M.; Marshall, A. R.; Schulz, P.; Suri, M.; Anderson, N. C.; Christians, J. A.; Nordlund, D.; Sokaras, D.; Kroll, T.*, et al.* Targeted Ligand-Exchange Chemistry on Cesium Lead Halide Perovskite Quantum Dots for High-Efficiency Photovoltaics. *J. Am. Chem. Soc.* **2018**, *140*, 10504-10513.
63. Brus, L. E. Electron--electron and electron-hole interactions in small semiconductor crystallites: The size dependence of the lowest excited electronic state. *J. Chem. Phys.* **1984**, *80*, 4403-4409.
64. Stoumpos, C. C.; Malliakas, C. D.; Peters, J. A.; Liu, Z.; Sebastian, M.; Im, J.; Chasapis, T. C.; Wibowo, A. C.; Chung, D. Y.; Freeman, A. J.*, et al.* Crystal Growth of the Perovskite Semiconductor CsPbBr3: A New Material for High-Energy Radiation Detection. *Crystal Growth & Design* **2013**, *13*, 2722-2727.
65. Yang, Z.; Wang, M.; Qiu, H.; Yao, X.; Lao, X.; Xu, S.; Lin, Z.; Sun, L.; Shao, J. Engineering the Exciton Dissociation in Quantum-Confined 2D CsPbBr3 Nanosheet Films. *Adv. Func. Mater.* **2018**, *28*, 1705908-10.
66. Yin, J.; Maity, P.; De Bastiani, M.; Dursun, I.; Bakr, O. M.; Brédas, J.-L.; Mohammed, O. F. Molecular behavior of zero-dimensional perovskites. *Sci. Adv.* **2017**, *3,* e1701793-8.
67. Brus, L. E. A simple model for the ionization potential, electron affinity, and aqueous redox potentials of small semiconductor crystallites. *J. Chem. Phys.* **1983**, *79*, 5566-5571.
68. Frederick, M. T.; Amin, V. A.; Cass, L. C.; Weiss, E. A. A Molecule to Detect and Perturb the Confinement of Charge Carriers in Quantum Dots. *Nano Lett.* **2011**, *11*, 5455-5460.
69. Beard, M. C.; Turner, G. M.; Murphy, J. E.; Micic, O. I.; Hanna, M. C.; Nozik, A. J.; Schmuttenmaer, C. A. Electronic Coupling in InP Nanoparticle Arrays. *Nano Lett.* **2003**, *3*, 1695-1699.
70. Crisp, R. W.; Schrauben, J. N.; Beard, M. C.; Luther, J. M.; Johnson, J. C. Coherent Exciton Delocalization in Strongly Coupled Quantum Dot Arrays. *Nano Lett.* **2013**, *13*, 4862-4869.
71. Bayer, M.; Hawrylak, P.; Hinzer, K.; Fafard, S.; Korkusinski, M.; Wasilewski, Z. R.; Stern, O.; Forchel, A. Coupling and Entangling of Quantum States in Quantum Dot Molecules. *Science* **2001**, *291*, 451-453.
72. Schedelbeck, G.; Wegscheider, W.; Bichler, M.; Abstreiter, G. Coupled Quantum Dots Fabricated by Cleaved Edge Overgrowth: From Artificial Atoms to Molecules. *Science* **1997**, *278*, 1792-1795.
73. Koole, R.; Liljeroth, P.; de Mello Donegá, C.; Vanmaekelbergh, D.; Meijerink, A. Electronic Coupling and Exciton Energy Transfer in CdTe Quantum-Dot Molecules. *J. Am. Chem. Soc.* **2006**, *128*, 10436-10441.
74. Boev, V. I.; Filonovich, S. A.; Vasilevskiy, M. I.; Silva, C. J.; Gomes, M. J. M.; Talapin, D. V.; Rogach, A. L. Dipole–dipole interaction effect on the optical response of quantum dot ensembles. *Physica B: Condensed Matter* **2003**, *338*, 347-352.

75. Teunis, M. B.; Dolai, S.; Sardar, R. Effects of Surface-Passivating Ligands and Ultrasmall CdSe Nanocrystal Size on the Delocalization of Exciton Confinement. *Langmuir* **2014**, *30*, 7851-7858.
76. Teunis, M. B.; Nagaraju, M.; Dutta, P.; Pu, J.; Muhoberac, B. B.; Sardar, R.; Agarwal, M. Elucidating the role of surface passivating ligand structural parameters in hole wave function delocalization in semiconductor cluster molecules. *Nanoscale* **2017**, *9*, 14127-14138.
77. Leatherdale, C. A.; Bawendi, M. G. Observation of solvatochromism in CdSe colloidal quantum dots. *Phys. Rev. B* **2001**, *63*, 165315-6.
78. Lee, D.; Sin, D. H.; Kim, S. W.; Lee, H.; Byun, H. R.; Mun, J.; Sung, W.; Kang, B.; Kim, D. G.; Ko, H., *et al.* Singlet Exciton Delocalization in Gold Nanoparticle-Tethered Poly(3-hexylthiophene) Nanofibers with Enhanced Intrachain Ordering. *Macromolecules* **2017**, *50*, 8487-8496.
79. Talapin, D. V.; Shevchenko, E. V.; Murray, C. B.; Titov, A. V.; Král, P. Dipole−Dipole Interactions in Nanoparticle Superlattices. *Nano Lett.* **2007**, *7*, 1213-1219.
80. Ohara, P. C.; Leff, D. V.; Heath, J. R.; Gelbart, W. M. Crystallization of Opals from Polydisperse Nanoparticles. *Phys. Rev. Lett.* **1995**, *75*, 3466-3469.
81. Xia, X.; Yang, M.; Wang, Y.; Zheng, Y.; Li, Q.; Chen, J.; Xia, Y. Quantifying the Coverage Density of Poly(ethylene glycol) Chains on the Surface of Gold Nanostructures. *ACS Nano* **2012**, *6*, 512-522.
82. Dirin, D. N.; Cherniukh, I.; Yakunin, S.; Shynkarenko, Y.; Kovalenko, M. V. Solution-Grown CsPbBr3 Perovskite Single Crystals for Photon Detection. *Chem. Mater.* **2016**, *28*, 8470-8474.
83. Perry, J. L.; Reuter, K. G.; Kai, M. P.; Herlihy, K. P.; Jones, S. W.; Luft, J. C.; Napier, M.; Bear, J. E.; DeSimone, J. M. PEGylated PRINT Nanoparticles: The Impact of PEG Density on Protein Binding, Macrophage Association, Biodistribution, and Pharmacokinetics. *Nano Lett.* **2012**, *12*, 5304-5310.
84. Tang, Z.; Kotov, N. A. One-Dimensional Assemblies of Nanoparticles: Preparation, Properties, and Promise. *Adv. Mater.* **2005**, *17*, 951-962.
85. Silvera Batista, C. A.; Larson, R. G.; Kotov, N. A. Nonadditivity of nanoparticle interactions. *Science* **2015**, *350,* 1242477-10.
86. Frost, J. M.; Butler, K. T.; Brivio, F.; Hendon, C. H.; van Schilfgaarde, M.; Walsh, A. Atomistic Origins of High-Performance in Hybrid Halide Perovskite Solar Cells. *Nano Lett.* **2014**, *14*, 2584-2590.
87. Baranov, D.; Fiore, A.; van Huis, M.; Giannini, C.; Falqui, A.; Lafont, U.; Zandbergen, H.; Zanella, M.; Cingolani, R.; Manna, L. Assembly of Colloidal Semiconductor Nanorods in Solution by Depletion Attraction. *Nano Letters* **2010**, *10*, 743-749.
88. Srivastava, S.; Santos, A.; Critchley, K.; Kim, K.-S.; Podsiadlo, P.; Sun, K.; Lee, J.; Xu, C.; Lilly, G. D.; Glotzer, S. C., *et al.* Light-Controlled Self-Assembly of Semiconductor Nanoparticles into Twisted Ribbons. *Science* **2010**, *327*, 1355-1359.
89. Lee, D.; Donkers, R. L.; DeSimone, J. M.; Murray, R. W. Voltammetry and Electron-Transfer Dynamics in a Molecular Melt of a 1.2 nm Metal Quantum Dot. *J. Am. Chem. Soc.* **2003**, *125*, 1182-1183.
90. Long, J. W.; Kim, I. K.; Murray, R. W. Hybrid Redox Polyethers: Molecular Melts of Metalloporphyrins. *J. Am. Chem. Soc.* **1997**, *119*, 11510-11515.

TOC Graphic

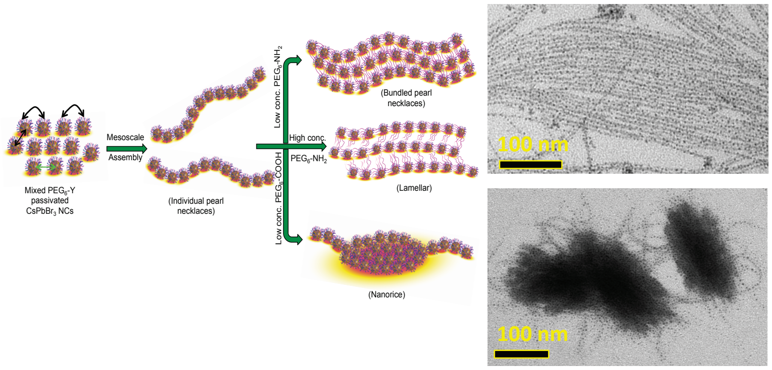
Mixed PEG6-Y passivated CsPbBr3 NCs
Mesoscale Assembly
(Individual pearl necklaces)
Low conc. PEG6-NH2
High conc. PEG6-NH2
Low conc. PEG6-COOH
(Bundled pearl necklaces)
(Lamellar)
(Nanorice)
100 nm
100 nm